Radiation Physics and Chemistry 239 (2026) 113403

Contents lists available at ScienceDirect

Radiation Physics and Chemistry

journal homepage: www.elsevier.com/locate/radphyschem

Experimental demonstration and quantitative analysis of X-ray-driven propulsion in graphene sponge

Weitong Yin [a], Zhiheng Xu [a,b,*], Xin Jin [a], Xiaobin Tang [a,b,**]

[a] Department of Nuclear Science and Technology, Nanjing University of Aeronautics and Astronautics, Nanjing, 211106, China
[b] Key Laboratory of Advanced Nuclear Technology and Radiation Protection, Ministry of Industry and Information Technology, Nanjing, 211106, China

ARTICLE INFO

Handling Editor: Dr. Chris Chantler

Keywords:
Radiation propulsion
Graphene sponge
X-ray-driven thrust
Vacuum effects
Propellant-free propulsion

ABSTRACT

This study presents the first experimental verification of X-ray-driven radiation propulsion in graphene sponges—distinct from conventional laser propulsion—establishing the fundamental mechanisms of radiation-matter interaction for propellant-free propulsion. To quantitatively characterize the thrust dynamics of graphene sponges, a lever-based pendulum setup (a device designed for precise measurement of microscale thrust) was employed under controlled conditions: vacuum pressure ranging from 0.06 to 100 kPa and X-ray tube voltage varying from 5 to 30 kV. Results show that the propulsive force increases monotonically with X-ray energy and exhibits a significant negative correlation with gas pressure. The maximum thrust of 32.73 μN (corresponding to a propulsion distance of 2.9 cm) was achieved at 30 kV/0.07 mA under a 0.06 kPa vacuum. The underlying interaction mechanisms differ by vacuum regime: In low-vacuum (10–100 kPa), thrust is dominated by gas-mediated energy transfer; while in high-vacuum (<1 kPa), it originates from direct X-ray interactions, including electron emission. Cyclic tests with 7-min intervals demonstrated a thrust recovery rate of 85 %–90 %, confirming the material's excellent reversibility in responding to radiation. This study establishes a fundamental framework of radiation physics and chemistry for radiation-driven propulsion, clarifying the characteristics of radiation energy absorption, conversion, and thrust output of graphene sponges under different pressure conditions. These findings provide a foundation for applying radiation-responsive graphene materials in propellant-free deep-space exploration.

1. Introduction

Current propulsion systems for space exploration are categorized into three principal classes: chemical propulsion (Shao et al., 2019; Kim and Cho, 2019; Dong et al., 2017; Budhwar et al., 2018), nuclear propulsion (Venneri and Eades, 2021; Kumar et al., 2025; Akimov et al., 2012), and photon propulsion (Wie and Murphy, 2007; Scholz et al., 2011; Gao et al., 2024; Fu et al., 2017). Conventional chemical propulsion rockets are constrained by inherently low payload fractions, with the propellant mass accounting for 70–90 % of the total vehicle mass, whereas the payload capacity typically accounts for approximately 5 % of the total mass. The inherently limited specific impulses and inferior energy densities of chemical propulsion systems impose fundamental constraints on their ability to perform long-range space missions (Xie et al., 2021; Stesina, 2019; Förster et al., 2020; Cline et al., 2024). Nuclear propulsion systems have demonstrated superior thrust-generation capabilities. However, their high initial investment costs and stringent regulatory requirements pose significant challenges for implementation (Park et al., 2022; Gustafson, 2021; Gabrielli et al., 2014). Despite its theoretical advantage of propellant-free operation via near-light-speed exhaust velocities, photon propulsion is hindered by the reliance of laser systems on bulky, power-intensive arrays and the susceptibility to energy loss from scattering/absorption in space environments (Swartzlander, 2022; Quarta and Mengali, 2023; Ma et al., 2017; Fu et al., 2016; Dubill and Swartzlander, 2021).

Recently, the interactions between lasers and graphene materials have been intensively investigated in the fields of photonics and materials science. For instance, Zhang et al. (2015) experimentally observed direct light propulsion in three-dimensional bulk graphene materials, demonstrating significant vertical displacement and rotational velocity under both watt-level laser irradiation and solar illumination while proposing a light-induced ejected electron mechanism. Wang et al.

* Corresponding author. Department of Nuclear Science and Technology, Nanjing University of Aeronautics and Astronautics, Nanjing, 211106, China.
** Corresponding author. Department of Nuclear Science and Technology, Nanjing University of Aeronautics and Astronautics, Nanjing, 211106, China.
E-mail addresses: xuzhiheng@nuaa.edu.cn (Z. Xu), tangxiaobin@nuaa.edu.cn (X. Tang).

https://doi.org/10.1016/j.radphyschem.2025.113403
Received 13 July 2025; Received in revised form 20 October 2025; Accepted 22 October 2025
Available online 24 October 2025

(2020) designed a laser-driven graphene sponge gravity pendulum and employed the optical lever method to perform quantitative measurements of opto-propulsive forces in laser-propelled graphene sponge (LPGS) systems. Their experimental results demonstrated a specific thrust of 62.6 mN/kW, a sub milliwatt laser power requirement (<7 mW), and fully reversible propulsion characteristics. These findings established the feasibility of using graphene-based materials for next-generation micro-propulsion devices, particularly for applications requiring continuous operation with minimal energy input.

Gaudenzi et al. (2020) experimentally demonstrated that graphene-based composites can significantly enhance the thrust generation of light sails under microgravity conditions through opto-thermal coupling mechanisms. Subsequent work by Wang et al. (2021) focused on the mechanistic analysis of LPGS, combining qualitative observations with quantitative measurements. Through comparative experiments under high-vacuum (0.002 Pa) and low-vacuum (6 Pa) conditions, the authors identified a laser-induced Knudsen force propulsion mechanism, wherein thermal gradients generated by laser absorption drove the momentum transfer via rarefied gas interactions. This mechanism establishes a theoretical foundation for optimizing the LPGS thrust efficiency across diverse pressure environments. Wang et al. (2023) reported the first macroscopic demonstration of the laser tractor effect in bulk graphene sponge materials achieved by irradiating a graphene-SiO_2 bilayer with a Gaussian laser beam. Using a precision torsion pendulum setup, they observed significant negative momentum transfer, showcasing the potential of the material for bidirectional propulsion control, which is a critical advancement for microscale attitude adjustment in space applications. Rao et al. (2024) reported a novel optical-propulsion metastructure strategy using metal-organic frameworks to generate graphene-metal metastructures (GMM) for pulsed laser micropropulsion (PLMP). Using a torsion pendulum setup, they systematically characterized the PLMP performance of GMM-(HKUST-1) and demonstrated a specific impulse of 1072.9 s, an ablation efficiency of 51.2 %, and an impulse thrust per mass of 105.2 μN μg^{-1}, surpassing traditional propellants. With an average particle size of ≈12 nm and a density of 0.958 g cm^{-3}, these metastructures exhibit 99 % light absorption efficiency and maintain stability under atmospheric and humid conditions, highlighting their potential for revolutionizing microspacecraft propulsion and energy systems.

In deep-space missions, laser-driven propulsion faces two core limitations that severely restrict its practical application: on the one hand, remote laser transmission suffers from significant energy decay and delay; on the other hand, self-contained laser sources require solving critical issues such as excessive weight, inefficient heat dissipation, and limited energy storage—all of which hinder their use in interstellar navigation. By contrast, X-rays, as a propulsion excitation source, possess key advantages that lasers cannot match: they exhibit superior penetrability, which allows them to effectively avoid the energy loss caused by scattering and absorption during transmission. Such X-rays can be supplied by radioactive isotopes, which offer additional advantages for deep-space scenarios: radioactive isotopes release energy through self-decay, requiring no external fuel replenishment; their decay process is immune to external environmental interference; and their output power decays slowly over time in a precisely predictable manner (Tavares and Terranova, 2023; Li et al., 2024). This makes them a stable energy solution for long-duration deep-space missions. However, a clear research gap exists in the current field: while laser-driven propulsion based on graphene sponges has been extensively studied and validated, X-ray-driven radiation propulsion using graphene materials has not yet been experimentally demonstrated.

To fill the aforementioned research gap, this study experimentally investigates the X-ray-driven propulsion of graphene sponges under a range of vacuum pressures and X-ray energies, comparing direct X-ray and radioluminescent photon excitation. The study conducted propulsion force measurements under a broad vacuum range (0.06–100 kPa) and X-ray tube voltages (5–30 kV) and found that under near-vacuum conditions (0.06 kPa), X-ray-driven propulsion achieves a maximum thrust of 32.73 μN at 30 kV/0.07 mA. In addition, the study performed sustainability tests for the continuous switching of excitation sources, which lays the groundwork for X-ray-driven graphene propulsion as a viable alternative to laser-based systems for microspacecraft.

2. Experimental section

2.1. Preparation of the graphene sponge pendulum

The graphene material, specifically a centimeter-scale bulk graphene sponge (Fig. S1, the detailed information can be found in Supporting Information) with a density of 17 mg/cm^3, was supplied by XFNANO (a commercial vendor). This material is a 3D crosslinked porous graphene with partial oxygen incorporation, featuring a hierarchical pore structure and an ultrahigh specific surface area. The microstructure afforded abundant adsorption sites and reactive centers (Fig. S2). A small amount of flake graphene was extracted from the bulk graphene sponge (diameter: 1 cm, height: 1.8 cm, total mass: 50 mg), fixed onto a 1.2 cm polypropylene film, and suspended using a non-conductive polyester fiber thread (length: 6.6 cm, diameter: 0.2 mm). Finally, the fabricated graphene-sponge pendulum was clamped to a holder. Once mounted on the pendulum suspension, the sample is hereafter referred to as the graphene sponge pendulum. The total mass of the graphene sponge pendulum was no greater than 10 mg, enabling significant and observable motion enhancement under radiation due to the reduced inertia facilitating more pronounced response to the applied radiation force. The reflectivity of the graphene sponge pendulum is approximately 5 % (Fig. S3) at laser wavelengths of 400–800 nm with a transmittance of less than 20 %, resulting in an absorbance of approximately 75 % at 400–800 nm, as determined using a UV–Vis–NIR spectrophotometer. An acrylic vacuum chamber coupled with a vacuum pump provided a vacuum environment, and the vacuum pressure was monitored using a digital vacuum gauge.

2.2. Propulsive force measurement methods for graphene sponge pendulum

A fixed graphene-sponge pendulum was placed inside the vacuum chamber and aligned collinearly with the emission port of the X-ray tube, as shown in Fig. 1a. In the second configuration, a gadolinium aluminium gallium garnet (GAGG) scintillator—selected for its high light output and short decay time, and used to convert X-ray energy into visible photons for radioluminescent propulsion measurements—was mounted on the inner wall of the vacuum chamber to ensure collinearity between the X-ray tube, GAGG scintillator, and graphene sponge pendulum (Fig. 1b).

The experimental test platform was composed of an X-ray tube, vacuum chamber, laser range finder and a camera system. A high-vacuum experimental environment was maintained using a two-stage vacuum pump to achieve a high vacuum. Fig. 2a illustrates the internal structure of the vacuum chamber. The internal air pressure was adjusted by controlling the operating time of the vacuum pump and monitoring the vacuum gauge, thereby enabling investigation of the effects of different air pressure environments. A smartphone camera positioned outside the chamber recorded the motion of the pendulum through a transparent observation window. A millimeter-scale ruler was placed behind the graphene sponge pendulum. The horizontal displacement changes were recorded via video recording, and the displacement values at every 0.1 s were measured using a laser rangefinder (Fig. 2b). Using data from video playback and laser rangefinder measurements, the displacement changes at specific time points were determined to calculate the magnitude of the propulsive force. The X-ray tube was located on the far-left side of the camera system (Fig. 2c). The radiation power intensity was regulated by controlling the voltage of the X-ray tube, enabling exploration of the effects of different radiation

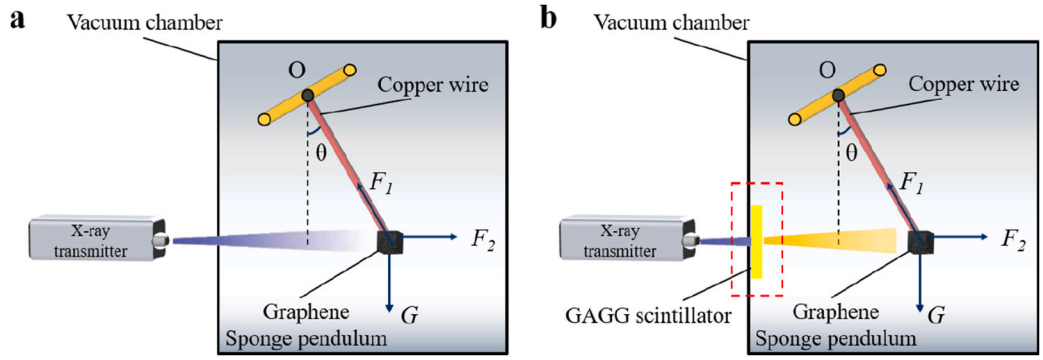

Fig. 1. Propulsion configurations of the graphene sponge pendulum under dual excitation modes: (a) direct X-ray irradiation setup, where the graphene sponge pendulum is aligned collinearly with the X-ray tube (emission port) inside the vacuum chamber; (b) radioluminescent photon excitation, utilizing a GAGG scintillator mounted on the vacuum chamber inner wall to convert X-ray energy into visible photons (475–675 nm).

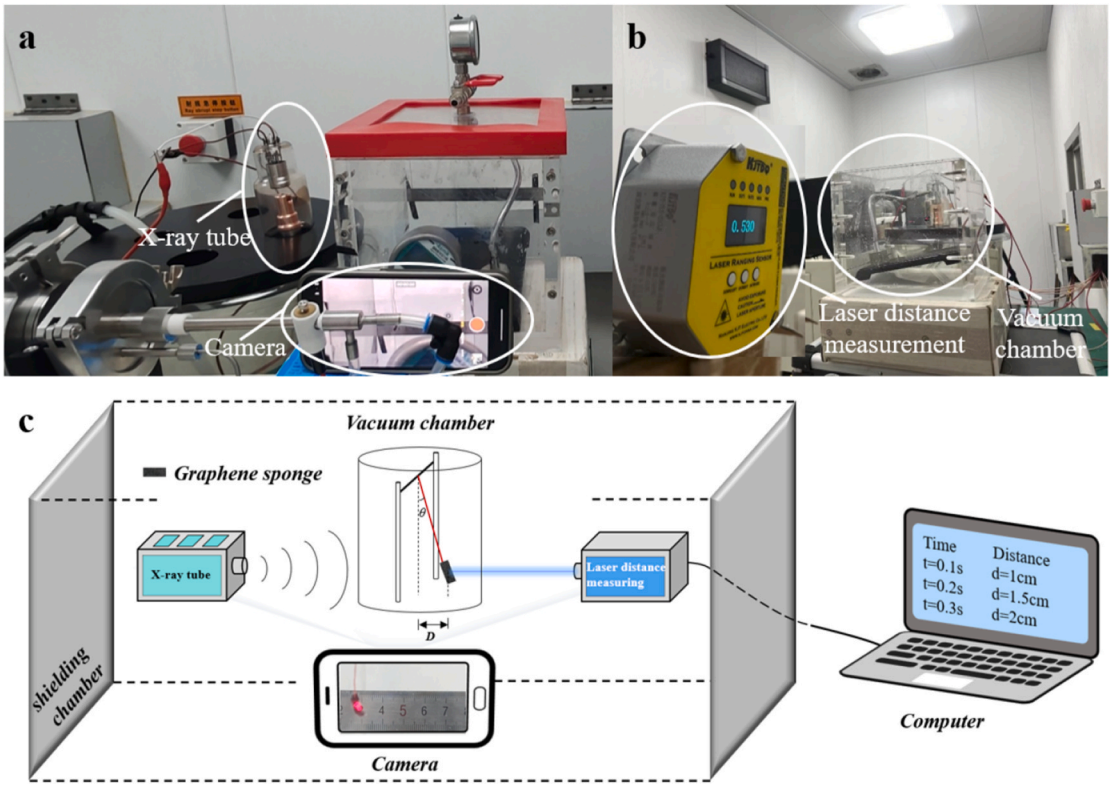

Fig. 2. Experimental facilities enabling effective radiation shielding and arbitrary air pressure control: (a) photograph of the X-ray tube, vacuum chamber structure, and graphene-sponge pendulum mounted on the stage inside the vacuum chamber; (b) image of the laser distance measurement instrument recording the real-time position of the graphene-sponge pendulum; (c) schematic diagram of the radiation-driven graphene-sponge pendulum experiment.

intensities. The voltages of the X-ray tube were set at 5, 10, 15, 20, 25, and 30 kV, and the vacuum levels were controlled at 100, 80, 60, 40, 20, and 0.06 kPa. The radioluminescence spectrum of the GAGG scintillator under X-ray excitation ranged from 475 to 675 nm (Fig. S4), which was measured using a fluorescence spectrophotometer (manufactured by Agilent Technologies, USA, with a measurement range of 200–900 nm and a wavelength measurement accuracy of ±1.5 nm). The X-ray energy spectrum spanned from 10 to 50 keV and was measured using an X-ray detector (XR-100SDD). A smartphone was used to record the entire propulsion process. To ensure radiation safety, all the experiments were conducted inside a lead-lined enclosure with real-time videos captured through the radiation-shielded viewing port of the chamber.

3. Results and discussion

3.1. Effect of distance between excitation source and graphene sponge pendulum on propulsion force

The X-ray tube voltage was set to 30 kV with a corresponding tube current of 0.07 mA, and the vacuum pressure was adjusted to 0.4 kPa. The vacuum chamber had a thickness of 2 cm, with 3 cm between the inner wall and graphene material. The distance between the X-ray tube and the outer wall of the vacuum chamber was varied from 7 to 15 cm to observe the propulsion force changes, and a lever method was used to measure the micro-thrust approximately. When the X-ray irradiated the graphene sponge pendulum on the left, propulsion occurred, causing a small deflection angle. Assuming that the graphene sponge pendulum behaves as a gravity pendulum and reaches a static equilibrium under X-

ray propulsion, the deflection angle θ becomes stable. The X-ray propulsion force was determined using the following equation:

$$F_2 = G\tan\theta = mg\tan\theta = mg\tan\cdot\left(\arcsin\frac{l}{x}\right) \quad (1)$$

where G is the total gravitational force acting on the graphene sponge pendulum, F_2 is the X-ray-induced propulsion force, l represents the distance from the suspension point to the center of mass of the pendulum, and x denotes the horizontal displacement of the pendulum from its equilibrium position. m, g, and l were predetermined prior to the experiments, allowing the propulsion force to be calculated solely from the measured horizontal displacement x. A scale was fixed to the back of the vacuum chamber, and x was measured at each time interval using both video playback and a laser rangefinder. The thrust value was obtained by substituting x into Equation (1).

Prior to X-ray irradiation, the graphene sponge pendulum was stably positioned on the left side of the vacuum chamber with no gas flow (Fig. 3a). Irradiation was initiated at t = 20 s for a duration of 2.5 min. The graphene sponge pendulum exhibited a significant rightward displacement along the irradiation direction, reaching its maximum displacement within 20 s post irradiation (Fig. 3b). This dynamic process is further illustrated in Supplementary Video 1, which shows the graphene sponge pendulum slowly moving left under irradiation.

The graphene sponge pendulum in a low-pressure vacuum chamber (pressure: 0.6 kPa) generated a measurable propulsive force under X-ray irradiation. Fig. 4a presents the temporal evolution of the horizontal displacement at varying distances r between the X-ray tube and the pendulum. At r = 14 cm, the maximum displacement reached 2.9 cm, corresponding to a propulsive force of 32.73 μN calculated via Equation (1). Here, m = 10 mg (graphene-sponge pendulum mass), g = 9.7949 m/s^2 (local gravitational acceleration), and L = 6.6 cm (pendulum arm length). Fig. 4b shows the force–distance relationship, revealing an optimal irradiation distance of 14 cm. The propulsive force initially increased and then decreased with increasing irradiation distance r.

Over time, the propulsion phenomena were observed at different distances r, As r increases, the position of the graphene sponge pendulum transitions from near the left container wall to the center of the container, and finally near the right container wall. Relatively stationary gas boundary layers are formed near the surfaces of both the graphene sponge pendulum and container walls. The boundary layers are thinner at shorter distances. The gas exchange must first traverse the boundary layer, and thinner boundary layers impose less resistance to gas diffusion, facilitating easier passage of gas molecules and enhancing the gas exchange between the object and container walls. Thus, at r = 14 cm, the distance likely achieved an optimal gas exchange equilibrium with all inner wall surfaces. Both excessively short and long distances resulted in insufficient thrust. However, in all cases tested so far, the thrust curves obtained show a trend of first increasing and then decreasing with the change of r.

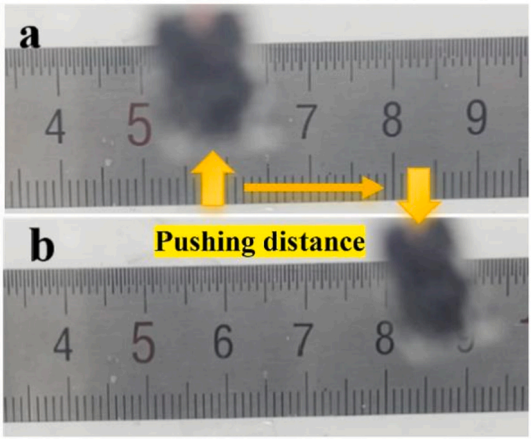

Fig. 3. Schematic of the graphene sponge pendulum (a) before excitation, (b) at the position of maximum propulsion displacement.

3.2. Propulsion performance of X-ray and radioluminesce photon under variable radiation intensity and gas pressure

To investigate the pressure and radiation intensity-dependent propulsion mechanisms, the vacuum chamber pressure was regulated from 0.06 kPa to 100 kPa, whereas the X-ray tube voltage was varied between 5 kV and 30 kV. Two parallel test configurations were employed to distinguish different excitation modes: one for direct X-ray propulsion and another for radioluminesce photon-induced propulsion (using a GAGG scintillator). Specifically, the GAGG scintillator was explicitly used to convert incident X-rays into radioluminesce photons, enabling the independent study of propulsion driven by such converted photons. As shown in Fig. 5a, the propulsive force exhibited a monotonically increasing trend with the X-ray tube voltage under all tested pressures, while demonstrating a strong inverse correlation with the gas density. For example, under X-ray excitation, when the vacuum level rises from 100 kPa to 0.06 kPa, the maximum thrust increases from near zero to 32.73 μN, exhibiting a clear positive correlation. Under radioluminesce photon excitation, with 5 kV, the improvement in thrust at 0.06 kPa versus that at 100 kPa reaches 1300 %, whereas with 30 kV, the corresponding improvement at 0.06 kPa versus that at 100 kPa is 501 % (Fig. 5b).

Critically, at near-vacuum conditions (0.06 kPa), X-ray-driven propulsion achieves a maximum thrust of 32.73 μN at 30 kV/0.07 mA. At pressures close to atmospheric pressure (80–100 kPa), frequent gas molecular collisions thicken the boundary layer, impeding momentum transfer and causing thrust decline; even at high tube voltages, the gas resistance becomes too large to enable effective propulsion. Although the specific propulsion mechanisms are still under investigation. It was hypothesized that the thrust may arise from electron ejection or gas-mediated energy transfer. Under high-vacuum conditions, where gas molecules are extremely sparse, radiation energy primarily generates thrust via direct material interactions (such as electron ejection). The increase in tube voltage has a limited gain for momentum transfer in the rarefied gas, leading to thrust saturation. In low-vacuum environments, thrust is dominated by the coupling of radiation excitation and gas molecular interactions, and higher tube voltages synergistically enhance both mechanisms. By contrast, high-vacuum thrust relies on the direct material response, with the tube voltage effects approaching linearity and exhibiting stable but moderate increases. Notably, radiation-driven propulsion generates measurable thrust across a broad pressure range (0.06–100 kPa), in stark contrast to laser-driven systems, which only produce thrust at 0.1–1 kPa due to severe energy losses from scattering and absorption in denser gases. This wide operational envelope highlights the unique adaptability of radiation propulsion to diverse space environments.

3.3. Stability and sustainability of radiation-driven propulsion

Using the same experimental setup, this study investigated the cyclic performance of a graphene sponge pendulum driven by X-ray excitation, with real-time video tracking of the pendulum position and dynamic thrust calculation at 10-s intervals. First, the continuous switching of the X-ray tube (tube voltage: 30 kV, tube current: 0.033 mA) was applied to irradiate the pendulum. The X-ray irradiation was initiated at t = 30 s and followed a cyclic protocol: 1 min irradiation → 30 s off → 1 min irradiation. The pendulum exhibited continuous actuation during these cycles. Subsequently, a 7-cycle continuous switching test was conducted to validate the sustained performance.

As shown in Fig. 6, under 0.06 kPa vacuum, the first irradiation (t = 0–60 s) generated an immediate 26.44 μN thrust, stabilizing at a

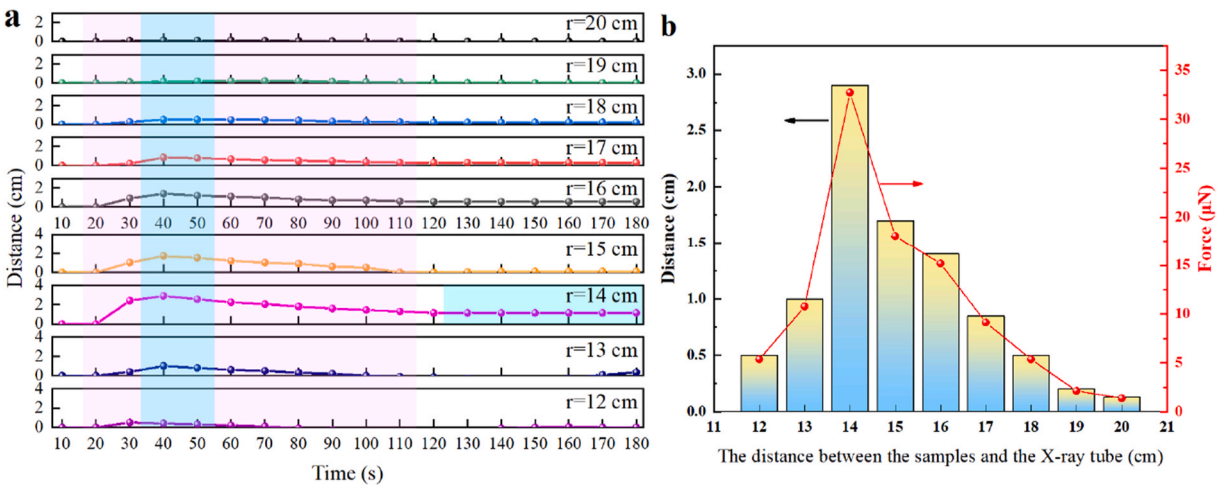

Fig. 4. (a) Horizontal displacement curves as a function of time at varying distances from the graphene sponge pendulum. (b) Maximum horizontal displacement and propulsive force as a function of distance from the graphene sponge pendulum.

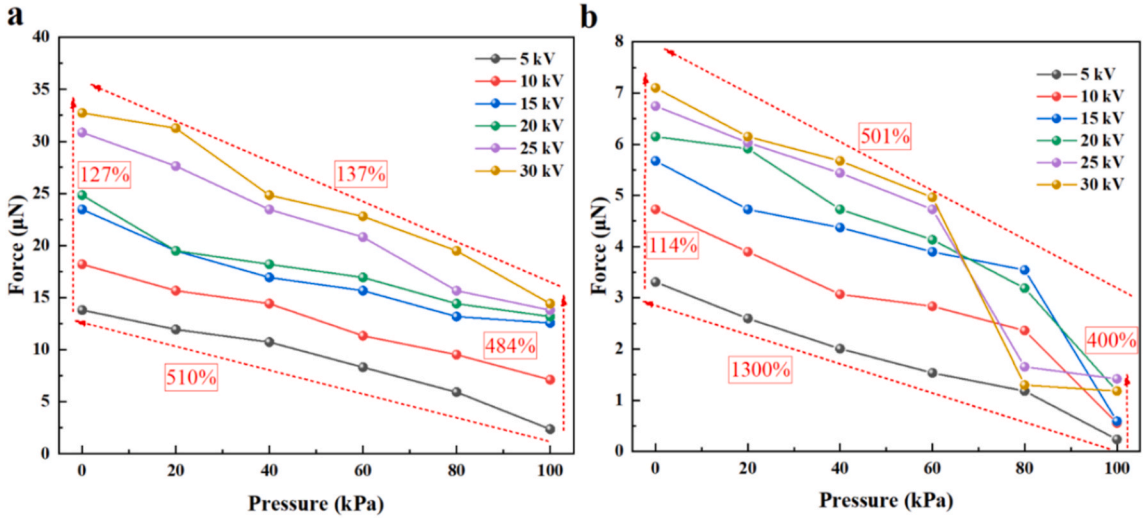

Fig. 5. Radiation-driven propulsion with varying gas pressures and power levels: (a) under X-ray excitation, (b) under radioluminesce photon excitation. (In both subfigures, solid curves (color-coded: black = 5 kV, red = 10 kV, blue = 15 kV, green = 20 kV, light purple = 25 kV, mustard = 30 kV) depict the propulsive force as a function of gas pressure at different X-ray tube voltages. Orange dotted lines represent the thrust improvement trend for both X-ray and radioluminesce photon excitations, with annotated percentage values (e.g., 501 %, 137 %, 114 %, etc.) quantifying the magnitude of thrust enhancement relative to baseline conditions under corresponding pressure and excitation regimes.). (For interpretation of the references to color in this figure legend, the reader is referred to the Web version of this article.)

consistent displacement. With an increasing number of cycles, the thrust exhibited progressive decay (8–12 % per cycle), which was attributed to the gradual ionization loss of adsorbed gases on the graphene surface and material fatigue in the X-ray response. During the irradiation process, fluctuations within a range of ±5 % were primarily attributed to slight instability in X-ray output (corresponding to ±2 % voltage variation) and secondarily to the stochastic effects arising from collisions in the rarefied gas environment.

Notably, after irradiation (t = 60–90 s), the pendulum displacement did not return to zero immediately, but decayed slowly, likely because of secondary electron emission from the chamber walls or sustained momentum transfer from the ionized gas residuals. A 30-s recovery period restored 85–90 % of the initial thrust upon restart, indicating reversible behavior, although long-term decay necessitates surface modification or coating optimization for stability. The experiment was constrained to a maximum of 7 cycles owing to radiation safety constraints, but preliminary data showed that thrust decayed to 60 % of the initial value by approximately 8 min (t = 450 s), approaching the detection threshold for effective propulsion (<5 μN). At this point, the thrust remained above 5 μN, demonstrating sustained functionality within the operational range. The experiment confirmed that the immediacy of the X-ray excitation—pendulum response was initiated within 2 s of activation and decayed within 5 s of shutdown, confirming that the thrust originates solely from real-time irradiation.

3.4. Broad implications and practical applicability of radiation-driven propulsion

The demonstrated stability, reversibility, and pressure-dependent propulsion of the graphene sponge pendulum under X-ray and radioluminescent excitation indicate that such materials can provide reliable, lightweight thrust in diverse space environments. Traditional chemical propulsion is limited by high propellant mass fractions (70–90 % of total mass) and low payload capacity, while laser-driven systems rely on bulky power arrays or remote transmission with significant energy decay. In contrast, X-ray excitation of graphene sponges requires no

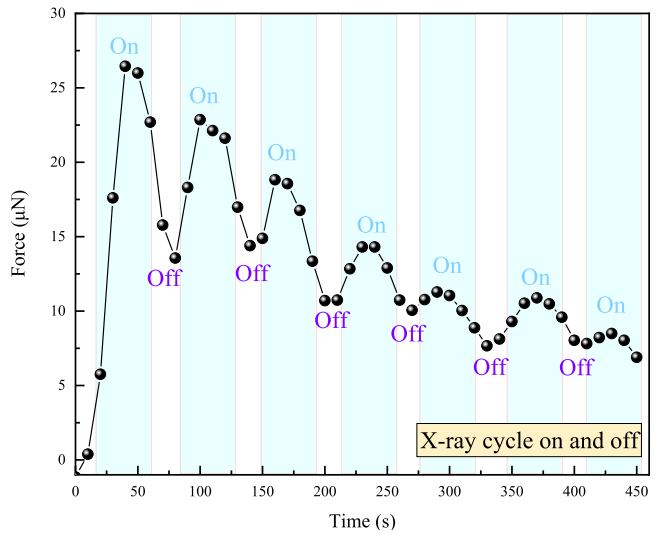

Fig. 6. Propulsive force curves obtained with the X-ray tube set at 30 kV and 0.07 mA and continuously switched as the excitation source at a pressure of 0.06 kPa.

propellant, and X-ray sources (e.g., radioactive isotopes) can provide stable, long-term energy via self-decay—eliminating the need for external fuel replenishment or complex heat dissipation systems. This makes technology well-suited for miniaturized space platforms, such as CubeSats or nanosatellites, which demand continuous, low-power thrust for attitude adjustment, orbital maintenance, or interplanetary trajectory corrections. Furthermore, the observed energy conversion mechanisms suggest potential applications in radiation-driven energy-harvesting devices, expanding the scope of these materials beyond propulsion alone.

4. Limitations

To ensure scientific transparency and guide future research, key limitations of this study are summarized as follows: Experiments relied on a single batch of commercial graphene sponge. Batch-to-batch differences in density, pore distribution, and surface oxygen content—factors that may affect gas adsorption and electron emission efficiency—were not explored, limiting the generalizability of results. The experiments were conducted with a centimeter-scale pendulum; performance at larger scales or different geometries is unknown. Extreme space-like vacuum conditions were simulated, but critical deep-space factors (temperature fluctuations, cosmic radiation, microgravity) that may alter thrust mechanisms were not considered. Thrust calculations relied on video tracking, laser rangefinders and additional uncertainty from X-ray voltage fluctuations. Cumulative errors may affect the precision of quantitative results. Only 7 short-term cycles were tested. Conclusions about prolonged operational stability are restricted.

5. Conclusions

This study first experimentally demonstrates X-ray-driven radiative propulsion in graphene sponges, including the observed thrust dependence on vacuum pressure and X-ray energy, directly demonstrates the feasibility of using these materials for propellant-free micropropulsion, overcoming limitations of conventional laser or chemical systems, and provides a platform for propellant-free radiation-driven micropropulsion and energy conversion technologies. Key findings: Performance-wise, thrust increases monotonically with X-ray energy (5–30 kV) and negatively correlates with pressure (0.06–100 kPa), peaking at 32.73 μN under 30 kV/0.07 mA and 0.06 kPa. Under radioluminescent excitation, the thrust enhancement ratio (0.06 vs 100 kPa) attenuates ~2.6-fold with increasing voltage, reflecting differing radiation-material coupling efficiencies. Seven cyclic tests verify stability: 8–12 % per-cycle thrust attenuation, with 85–90 % recovery in 30 s, indicating good reversibility. These findings highlight their potential application in deep-space missions and energy conversion devices, where lightweight, efficient, and reversible propulsion is critical. By establishing both the mechanistic understanding and performance metrics, this study provides a foundation for designing microspacecraft and nanosatellites that leverage radiation-driven propulsion, bridging fundamental research with practical space applications. In the future, we plan to fabricate this material into thinner and lighter films, which will serve as sails for micro-spacecraft and be applied to both attitude control and overall propulsion of the spacecraft.

CRediT authorship contribution statement

Weitong Yin: Writing – original draft, Data curation, Conceptualization. **Zhiheng Xu:** Writing – review & editing, Supervision, Methodology, Funding acquisition, Formal analysis, Conceptualization. **Xin Jin:** Writing – review & editing. **Xiaobin Tang:** Writing – review & editing, Supervision, Methodology.

Declaration of competing interest

The authors declare that they have no known competing financial interests or personal relationships that could have appeared to influence the work reported in this paper.

Acknowledgements

This work was supported by the prospective layout project of Nanjing University of Aeronautics and Astronautics (Grant No. ILB240161A24). We acknowledge the Center for Microscopy and Analysis at Nanjing University of Aeronautics and Astronautics for the material characteristics analysis.

Appendix A. Supplementary data

Supplementary data to this article can be found online at https://doi.org/10.1016/j.radphyschem.2025.113403

Data availability

Data will be made available on request.

References

Akimov, V.N., Koroteev, A.A., Koroteev, A.S., 2012. Space nuclear power systems: yesterday, today, and tomorrow. Therm. Eng. 59, 953–959. https://doi.org/10.1134/S0040601512130022.

Budhwar, A.S., Gautam, A., More, P.V., Pant, C.S., Banerjee, S., Khanna, P.K., 2018. Modified iron oxide nanoparticles as burn rate enhancer in composite solid propellants. Vacuum 156, 483–491. https://doi.org/10.1016/j.vacuum.2018.08.013.

Cline, B.C., Parker, K.I., Rosales, J.J., Rovey, J.L., West, S.T., 2024. Lunar SmallSat missions with chemical-electrospray multimode propulsion. J. Spacecraft Rockets 61, 1032–1046. https://doi.org/10.2514/1.A35820.

Dong, R., Wang, C., Wang, Q., Pei, A., She, X., Zhang, Y., et al., 2017. ZnO-based microrockets with light-enhanced propulsion. Nanoscale 9, 15027–15032. https://doi.org/10.1039/c7nr05168a.

Dubill, A.L., Swartzlander Jr., G.A.J., 2021. Circumnavigating the sun with diffractive solar sails. Acta Astronaut. 187, 190–195. https://doi.org/10.1016/j.actaastro.2021.06.036.

Förster, D.J., Faas, S., Weber, R., Graf, T., 2020. Thrust enhancement and propellant conservation for laser propulsion using ultra-short double pulses. Appl. Surf. Sci. 510, 145391. https://doi.org/10.1016/j.apsusc.2020.145391.

Fu, B., Sperber, E., Eke, F., 2016. Solar sail technology-A state of the art review. Prog. Aero. Sci. 86, 19. https://doi.org/10.1016/j.paerosci.2016.07.001.

Fu, B., Gede, G., Eke, F.O., 2017. Controllability of a square solar sail with movable membrane tips. Proc. Inst. Mech. Eng. Part G-J. Aerosp. Eng. 231, 1065–1075. https://doi.org/10.1177/0954410016647533.

Gabrielli, R.A., Petkow, D., Herdrich, G., Laufer, R., Röser, H.P., 2014. Two generic concepts for space propulsion based on thermal nuclear fusion. Acta Astronaut. 101, 129–137. https://doi.org/10.1016/j.actaastro.2014.03.015.

Gaudenzi, R., Stefani, D., Cartamil-Bueno, S.J., 2020. Light-induced propulsion of graphene-on-grid sails in microgravity. Acta Astronaut. 174, 204–210. https://doi.org/10.1016/j.actaastro.2020.03.030.

Gustafson, J.L., 2021. Space nuclear propulsion fuel and moderator development plan conceptual testing reference design. Nucl. Technol. 207, 882–884. https://doi.org/10.1080/00295450.2021.1890991.

Gao, R., Kelzenberg, M.D., Atwater, H.A., 2024. Dynamically stable radiation pressure propulsion of flexible lightsails for interstellar exploration. Nat. Commun. 15, 4203. https://doi.org/10.1038/s41467-024-47476-1.

Kim, Y., Cho, J., 2019. Surface erosion analysis for thermal insulation materials of graphite and carbon-carbon composite. Appl. Sci.-Basel. 9, 3323. https://doi.org/10.3390/app9163323.

Kumar, S., Thomas, L.D., Cassibry, J.T., 2025. Application of nuclear thermal propulsion for sustainable cislunar exploration. Acta Astronaut. 228, 435–441. https://doi.org/10.1016/j.actaastro.2024.11.045.

Li, K., Yan, C., Wang, J., Zhu, K., Guo, J., Zhang, Y., et al., 2024. Micronuclear battery based on a coalescent energy transducer. Nature 633, 811–815. https://doi.org/10.1038/s41586-024-07933-9.

Ma, D., Murray, J., Munday, J.N., 2017. Controllable propulsion by light: steering a solar sail via tunable radiation pressure. Adv. Opt. Mater. 5, 1600668. https://doi.org/10.1002/adom.201600668.

Park, H.Y., Kang, Y.H., Soo, K.J., Yang, S.S., 2022. State of the art for space propulsion employing nuclear power. J. Korean Soc. Propuls. Eng. 26, 86–100. https://doi.org/10.6108/KSPE.2022.26.6.086.

Quarta, A.A., Mengali, G., 2023. Solar sail orbit raising with electro-optically controlled diffractive film. Appl. Sci.-Basel 13, 7078. https://doi.org/10.3390/app13127078.

Rao, S., Yi, W., Jiang, H., Zhang, S., Yi, J., Cheng, G., 2024. Optical-propulsion metastructures. Adv. Mater. 36, 2406384. https://doi.org/10.1002/adma.202406384.

Scholz, C., Romagnoli, D., Dachwald, B., Theil, S., 2011. Performance analysis of an attitude control system for solar sails using sliding masses. Adv. Space Res. 48, 1822–1835. https://doi.org/10.1016/j.asr.2011.05.032.

Shao, Y., Feng, X., Dai, L., Dodelet, J., 2019. Advancing materials electrochemistry for chemical transformation. Adv. Mater. 31, 284–311. https://doi.org/10.1002/adma.201903622.

Stesina, F., 2019. Validation of a test platform to qualify miniaturized electric propulsion systems. Aerospace 6, 99. https://doi.org/10.3390/aerospace6090099.

Swartzlander, G.A., 2022. Theory of radiation pressure on a diffractive solar sail. J. Opt. Soc. Am. B 39, 2556–2563. https://doi.org/10.1364/JOSAB.468588.

Tavares, O.A.P., Terranova, M.L., 2023. Physical viability for nuclear batteries. J. Radioanal. Nucl. Chem. 332, 3933. https://doi.org/10.1007/s10967-023-09034-9, 3342.

Venneri, P., Eades, M., 2021. Space nuclear power and propulsion at USNC-tech. Nucl. Technol. 207, 876–881. https://doi.org/10.1080/00295450.2021.1895662.

Wang, L., Tam, W.Y., Zhao, Q., Wang, X., 2020. Quantitative measurement and mechanism analysis of the high-efficiency laser propulsion of a graphene sponge. Opt. Express 28, 33869–33875. https://doi.org/10.1364/OE.403875.

Wang, L., Dai, M., Zhao, Q., Wang, X., 2021. Mechanism research of the laser propulsion of bulk graphene sponge material through high vacuum experiment. Vacuum 191, 110334. https://doi.org/10.1016/j.vacuum.2021.110334.

Wang, L., Wang, S., Zhao, Q., Wang, X., 2023. Macroscopic laser pulling based on the knudsen force in rarefied gas. Opt. Express 31, 2665–2674. https://doi.org/10.1364/OE.480019.

Wie, B., Murphy, D., 2007. Solar-sail attitude control design for a sail flight validation mission. J. Space Cr. Rockets 44, 809–821. https://doi.org/10.2514/1.22996.

Xie, Y., Savvarisal, A., Tsourdos, A., Zhang, D., Gu, J., 2021. Review of hybrid electric powered aircraft, its conceptual design and energy management methodologies. Chin. J. Aeronaut. 34, 432–450. https://doi.org/10.1016/j.cja.2020.07.017.

Zhang, T., Chang, H., Wu, Y., Xiao, P., Yi, N., Lu, Y., et al., 2015. Macroscopic and direct light propulsion of bulk graphene material. Nat. Photonics 9, 471–476. https://doi.org/10.1038/NPHOTON.2015.105.